Journal of Sedimentary Research

Journal of Sedimentary Research, 2022, v. 92, 445–459
Research Article
DOI: 10.2110/jsr.2021.062

PALEOHYDRAULIC ANALYSIS OF AN ANCIENT DISTRIBUTIVE FLUVIAL SYSTEM

ADRIAN J. HARTLEY[1] AND AMANDA OWEN[2]
[1]Department of Geology & Geophysics, University of Aberdeen, Aberdeen AB24 3UE, U.K.
[2]School of Geographical and Earth Sciences, University of Glasgow, Glasgow G12 8QQ, U.K.

ABSTRACT: **Reconstructing the paleohydraulics of ancient fluvial systems has important implications when determining channel-body dimensions in the subsurface as well as aiding source-to-sink studies and quantitatively determining the impact of changing climatic conditions. We undertake a paleohydraulic analysis of the Upper Jurassic Salt Wash distributive fluvial system (DFS) of the Morrison Formation, SW USA, to determine if downstream trends such as decreasing channel size and discharge, inferred in studies of DFS, are present. Channel depth was estimated using cross-set height values and preserved bar thickness. Nine localities across the exposed part of the Salt Wash system were studied. In total, 49 bars were measured, full bar thickness was determined from 12 complete bars, and average cross-set height was calculated for 37 bars. Estimates of maximum bankfull channel depth were derived from measured bar thicknesses. Bar height was then obtained and converted to mean bankfull channel depth using a shape adjustment factor of 0.65. The bar-derived mean bankfull channel depths were then used to derive a factor for which dune cross-set heights could be converted to mean bankfull channel depth (4.6) and maximum bankfull channel depth (7.1). These factors were then applied to localities where only cross-set height data were available, thus allowing consistent comparison and extrapolation of mean bankfull channel depth over the preserved DFS area. The use of measured bar thicknesses to calibrate estimates of mean channel depth from reconstructed dune heights is considered a useful approach, with the factor of 4.6 estimated here being lower than that (6 to 10) commonly used in comparable studies.**

The datasets for the Salt Wash DFS record systematic downstream trends in cross-set height, bar thickness, calculated channel depth, estimated channel width, and estimated Q, with variability and overlap between the proximal to medial, and medial to distal parts. The variability superimposed on the regional downstream trends is attributed to a combination of autocyclic processes such as variations in discharge, depth of scour, and avulsion as well as more regional-scale channel-belt switching together with allocyclic controls. The wide spatial distribution of the dataset in this study allows distinction between local autocyclic controls and regional downstream trends. Formative discharge shows no downstream trend across the entire Salt Wash DFS, with a wide range in coefficient of variation of preserved cross set thickness (CV(dst) values of 0.1 to 1.1) indicative of flashy (variable) discharge.

The spatial distribution of the Salt Wash dataset allows extrapolation of trends upstream to the unexposed part of the system that allows insights into the characteristics of the channel system in the apex area ($\sim$ 150 km to the southwest and removed by post depositional erosion). The fluvial system would have a mean depth of 9 m, and a bankfull-depth discharge of around 1450 m^3/s with mean cross-set heights of between 50 and 70 cm. These estimates are in line with those from present-day DFSs in the Himalayan and Andean foreland basins that have a scale similar to that estimated for the Salt Wash system.

INTRODUCTION

Reconstructing channel dimensions in ancient fluvial deposits allows constraints to be placed on the nature of the depositing river system, providing insights into paleohydrology and discharge. Once determined, paleodischarge can be used to quantify catchment-area sizes for ancient depositional systems using scaling relationships from modern systems (e.g., Davidson and North 2009; Bhattacharya et al. 2016). Accurate estimates of the paleohydraulics and dimensions of ancient river deposits can be used to enhance paleogeographic and paleoclimatic reconstructions for specific areas and time periods and provide constraints on sandstone body dimensions. This approach is important in determining the response of fluvial systems to climate-change events such as the Paleocene–Eocene Thermal Maximum (e.g., Foreman et al. 2012) and the Carnian Pluvial Event (Dal Corso et al. 2020) or changes in catchment size and/or elevation related to tectonic events (e.g., Wernicke 2011) or drainage capture (e.g., Mather 1993). An understanding of fluvial response to climate-change events may also help in predicting and mitigating the impacts of current anthropogenically induced climate warming on fluvial systems. In addition, establishing the likely controls on dimensions of fluvial channel bodies is important for the subsurface extraction of water (e.g., Weissmann et al. 2002; MacDonald et al. 2016; van Dijk et al. 2016), heat (e.g., Willems et

Published Online: May 2022

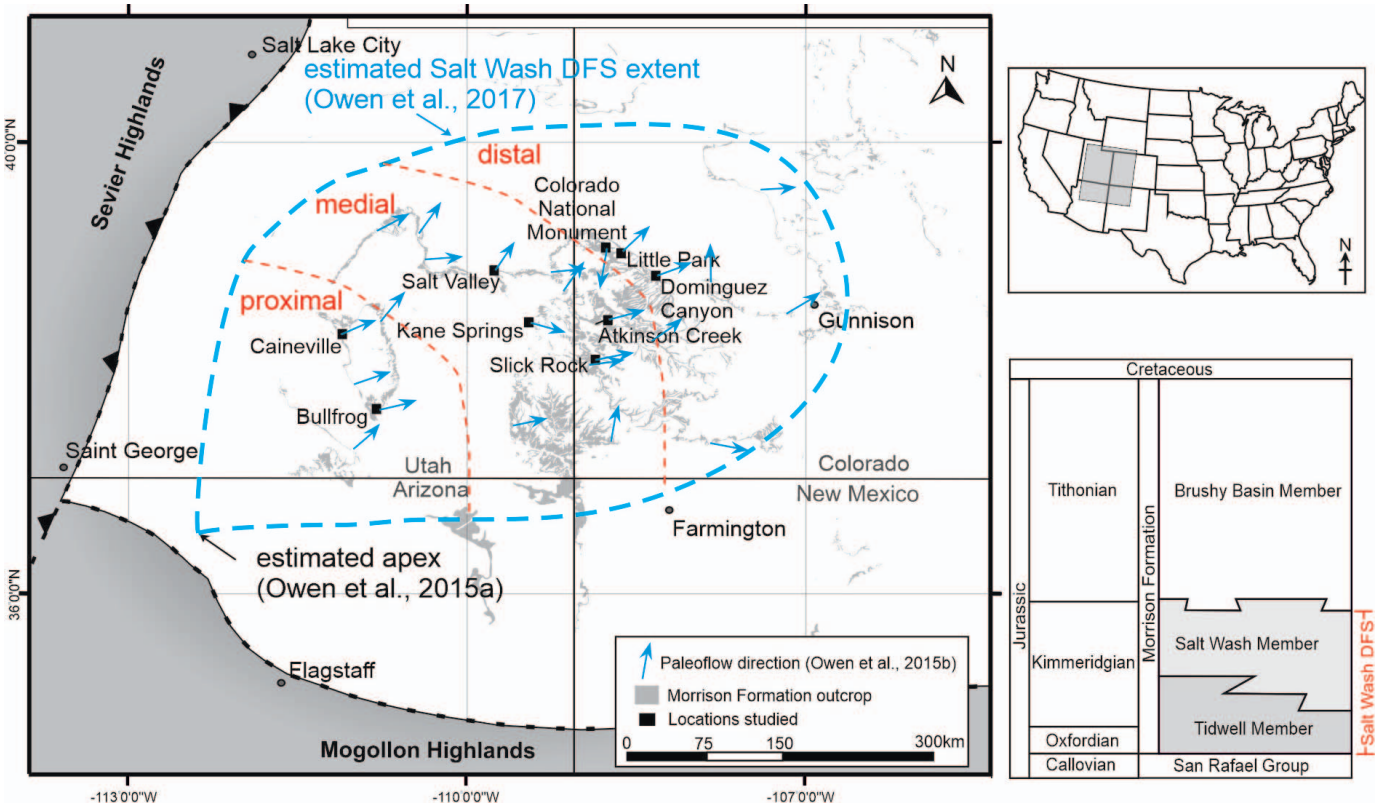

FIG. 1.—Paleogeographic map and stratigraphy of the Salt Wash fluvial system. Modified from Owen et al. (2015a, 2015b)

al. 2016) and hydrocarbons (e.g., Moscariello 2005; Keough et al. 2007) as well as the storage of greenhouse gases such as CO_2 (e.g., Lu et al. 2012).

The reconstruction of channel dimensions requires estimates of bankfull river depth (e.g., Bridge and Mackey 1993). This is computed from relationships between the thickness of the preserved channel fill and the depth of the depositing channel derived either from analysis of modern rivers (Allen 1965; Leeder 1973; Collinson 1978; Lorenz et al. 1985) or from data compilations (Fielding and Crane 1987; Mijnssen 1997). Estimates of bankfull channel depth of ancient channel deposits can be derived from the relationship between mean dune height and formative flow depth, although there is a large scatter (Yalin 1964; Allen 1982; Bridge and Tye 2000). Theoretical and empirical studies show a strong correspondence between the thickness of preserved cross-set strata and the height of the depositing subaqueous dunes (Leclair et al. 1997; Leclair and Bridge 2001; Leclair 2002). Studies of this kind make it possible to derive estimates of channel depth from cross-set thickness for ancient rivers that are consistent with more direct estimators such as bar thickness (Bridge and Tye 2000; Bhattacharya and Tye 2004; Adams and Bhattacharya 2005; McLaurin and Steel 2007).

This study aims to: 1) test the methodology for reconstructing bankfull depth from cross-set thickness using the approach of Leclair and Bridge (2001) by comparing channel-depth estimates with full bar thicknesses measured in the field and 2) test whether there is any spatial variability in paleohydraulic parameters across a near entire fluvial system. The Salt Wash distributive fluvial system (DFS) of the Upper Jurassic Morrison Formation, SW USA, was chosen to explore paleohydraulic relationships due to its well-established and quantified spatial context. The system was first identified and mapped by Craig et al. (1955) and Mullens and Freeman (1957) and subsequently built on and expanded by numerous authors (e.g., Tyler and Ethridge 1983; Peterson 1980 1984; Robinson and McCabe 1997; Turner and Peterson 2004; Kjemperud et al. 2008). Owen et al. (2015b) refined the extent of the system and quantified sedimentary characteristics. A downstream decrease in grain size (coarse sand to silt), amalgamated channel percentage (67–0%), channel body thickness (15–3.8 m), and geometry (from large, amalgamated complexes to isolated single story bodies) was identified with a concomitant increase in floodplain preservation (38–94%). These trends confirm the Salt Wash system to represent the deposits of a distributive fluvial system (DFS) (*sensu* Hartley et al. 2010; Weissmann et al. 2010, 2015). The apex of the system has been statistically modeled to lie in northwestern Arizona, with the source area located around the ancient Mogollon–Sevier Highlands syntaxis (Fig. 1; Owen et al. 2015a, 2015b). The system radiates from this apex position across southern and central Utah and western Colorado and covers an area of $\sim$ 100,000 km^2, with flow in a predominantly northeastern direction (Fig. 1; Peterson 1980, 1984; Kjemperud et al. 2008; Weissman et al. 2013; Owen et al. 2017). The Salt Wash DFS is 170 m thick in the proximal region and decreases in thickness to the northeast (downstream) to 50 m (Owen et al. 2015b). A detailed analysis of the internal stratigraphy of the unit was undertaken by Owen et al. (2017). These authors illustrated that whilst the Salt Wash system overall displays a progradational motif with a general upward increase in channel sandstone-body preservation and channel-body thickness and amalgamation, in detail there is considerable variation. For example, in most sections (61% of 23 sections) a clear progradational signature was observed, but in other areas a decrease in channel presence and thickness was observed (13%), whilst in 26% of the sections no obvious trends were present. The authors attributed this to variation in preservation potential across the system, associated with a combination of smaller-scale avulsion cycles, larger system-scale trends, and fluctuations in upstream controls such as climate and tectonics (Owen et al. 2017). In terms of the nature of the channels responsible for deposition of the Salt Wash fluvial system, early work based on grain size, dominance of cross stratification, and limited floodplain development

suggested that the predominant planform type was braided (Peterson 1984; Robinson and McCabe 1998). More recent analysis, utilizing detailed outcrop studies combined with high-resolution remotely sensed imagery (Hartley et al. 2015, 2018; Swan et al. 2018), has illustrated that a meandering planform style is dominant, with most of the outcrop belt comprising an amalgamated meander belt. Only in the most proximal part of the outcrop belt (e.g., Bullfrog, Fig. 1) is a mixed braided-meandering style inferred. The climate in the basin during Morrison Formation deposition in the Late Jurassic is understood to have been semiarid with seasonal precipitation similar to that of a modern African savannah (e.g., Turner and Peterson 2004; Demko et al. 2004; Owen et al. 2015b). During Morrison deposition, the western interior seaway was regressing towards present-day Canada, with the shoreline thought to be close to the USA–Canada border by the end of the Late Jurassic (Turner and Peterson 2004). It is thus postulated that backwater effects and associated downstream base-level changes had minimal influence on the sedimentation patterns in the Salt Wash fluvial system (Owen et al. 2017). As with many fluvial deposits, a detailed chronostratigraphic framework is not available for the Salt Wash succession.

The spatial context provided by previous studies and the established downstream and along-strike characteristics of the Salt Wash system allow the DFS model proposed by Weissmann et al. (2010, 2015) to be tested. These authors consider the downstream decrease in channel size and amalgamation to result from a reduction in discharge due to a combination of channel bifurcation, infiltration into a permeable substrate, and evapotranspiration. We seek to determine the downstream changes in channel dimensions by mapping the paleohydraulic properties of the Salt Wash channels at various sites across the DFS to gain a better understanding of the spatial variability of paleodischarge as well as the nature of the formative discharge (e.g., Leary and Ganti 2019).

METHODS

Channel-Depth Estimation

Channel depth and paleohydraulic parameters were calculated for each of the nine locations studied using standard methods (e.g., Bridge and Mackey 1993; Leclair and Bridge 2001). Channel depth was reconstructed using the approach outlined by Leclair and Bridge (2001), although it is noted that this provides a broad estimate and that more recent studies have highlighted that a range of relationships between dune height and flow depth are present (Bradley and Venditti 2017, 2019; Cisneros et al. 2020). Preserved trough cross-strata set height was measured in a vertical profile for 49 bars across the study area (Figs. 2, 3). Full bar thickness (T_b in Fig. 3C) was determined for 12 bars where complete preservation and exposure allowed, the remaining 37 bars are referred to as incomplete. Bars were considered complete where they graded upwards into bar-top or abandoned-channel deposits such as rippled sandstones or mudstones. Bars where cross-stratified sandstones were truncated beneath an erosion surface overlain by younger channel-fill deposits were considered incomplete. Vertical stratigraphic height was noted for all studied bars and mapped onto sedimentary logs presented by Owen et al. (2015b) to provide both vertical and spatial context (Fig. 2).

Only compound bars where the number of sets was greater than five were included in the analysis. Abnormally thick, isolated cross-sets formed by unit bars were excluded from the dataset because they would provide an overestimate of channel depth. Bars with highly truncated thalweg sets at the base were not measured. Preserved cross-set height was decompacted (factor of 10%; Leclair and Bridge 2001) and used to calculate mean dune height (H_m) using the equation

$$H_m = 2.9(\pm\ 0.7) \tag{1}$$

mean cross-set thickness (Leclair and Bridge 2001).

With mean bankfull channel depth (*D)* calculated using Leclair and Bridge (2001):

$$D_{mean} = (6 - 10)H_m \tag{2}$$

The wide range of factors required to determine mean bankfull channel depth is due to the large scatter in the measured relationship between mean dune height and the flow depth to form dunes (Yalin 1964; Allen 1982; Bridge and Tye 2000). To mitigate this uncertainty, we calibrated estimates of mean channel depth derived from cross-set heights against maximum channel depth determined from known bar thickness (n = 12 from all localities excluding Salt Valley, where a fully preserved bar was not observed) (Fig. 3C). This allowed the independent calculation of the correction factors used to determine depth from dune heights. Bar thickness (T_b in Fig. 3C) is taken to approximate bar height (H_b in Fig. 3C). We applied a decompaction factor of 10% to H_b. An additional factor of 20% was applied subsequently, as bar height is considered to represent approximately 80% of maximum bankflow depth (e.g., Bridge 2003):

$$D_{max} = (H_b \div 0.9) \div 0.8 \tag{3}$$

Conversion from maximum bankfull depth to mean bankfull depth utilized the shape adjustment factor of 0.65 used by Bridge and Mackey (1993):

$$D_{mean} = 0.65D_{max} \tag{4}$$

To determine the correction factor needed to ascertain depth from dune height, the bar-derived mean bankfull flow depth is divided by H_m:

$$\text{Correction factor} = D_{mean(bar)}/H_m \tag{5}$$

The range of correction factors needed to determine the mean bankfull flow depth from incomplete bar thicknesses ranged from 2.0 (227 km downstream; Caineville) to 8.23 (333 km downstream; Kane Springs) (Fig. 4; Table 1). Similarly, the range of factors needed to ascertain the measured maximum bankfull depth ranged from 3.1 (Caineville) to 12.7 (Kane Springs).

The large range in both maximum and mean bankfull flow depths may be due to variations in the stratigraphic level and lateral position in the Salt Wash system from which each bar was measured. The largest factors for mean bankfull flow depth (8.2 at 333 km downstream, Kane Springs; 6.5 at 433 km downstream, Little Park) were located towards the top of the studied sections in the most progradational (relatively proximal) part of the succession. The lowest value (2) is located towards the base of the section at Caineville (227 km downstream) in the more proximal region of the studied sections.

The variability in mean and maximum bankful flow depth is to be expected in a highly avulsive system. Due to this variation, we calculated a mean for all factors needed across the system. For our whole dataset it was found that on average a factor of 4.64 was required to accurately predict mean bankfull depth (*D)* and 7.14 to predict maximum bankfull depth (Table 1). *D* was then calculated for all localities using the factors calculated here and the minimum (6) and maximum (10) factors of Leclair and Bridge such that a comparison could be made (Fig. 5).

Paleohydraulics

To obtain paleodischarge the channel depth, cross-sectional area and flow velocities must be estimated. Mean channel depth is determined using the modified reconstructed-dune-height method of Leclair and Bridge (2001) or the thickness of preserved bars using the methodologies outlined above (Table 2). Cross-sectional area is determined by multiplying the paleochannel depth by width with an adjustment factor of 0.65 for the channel shape (Bridge and Mackey 1993):

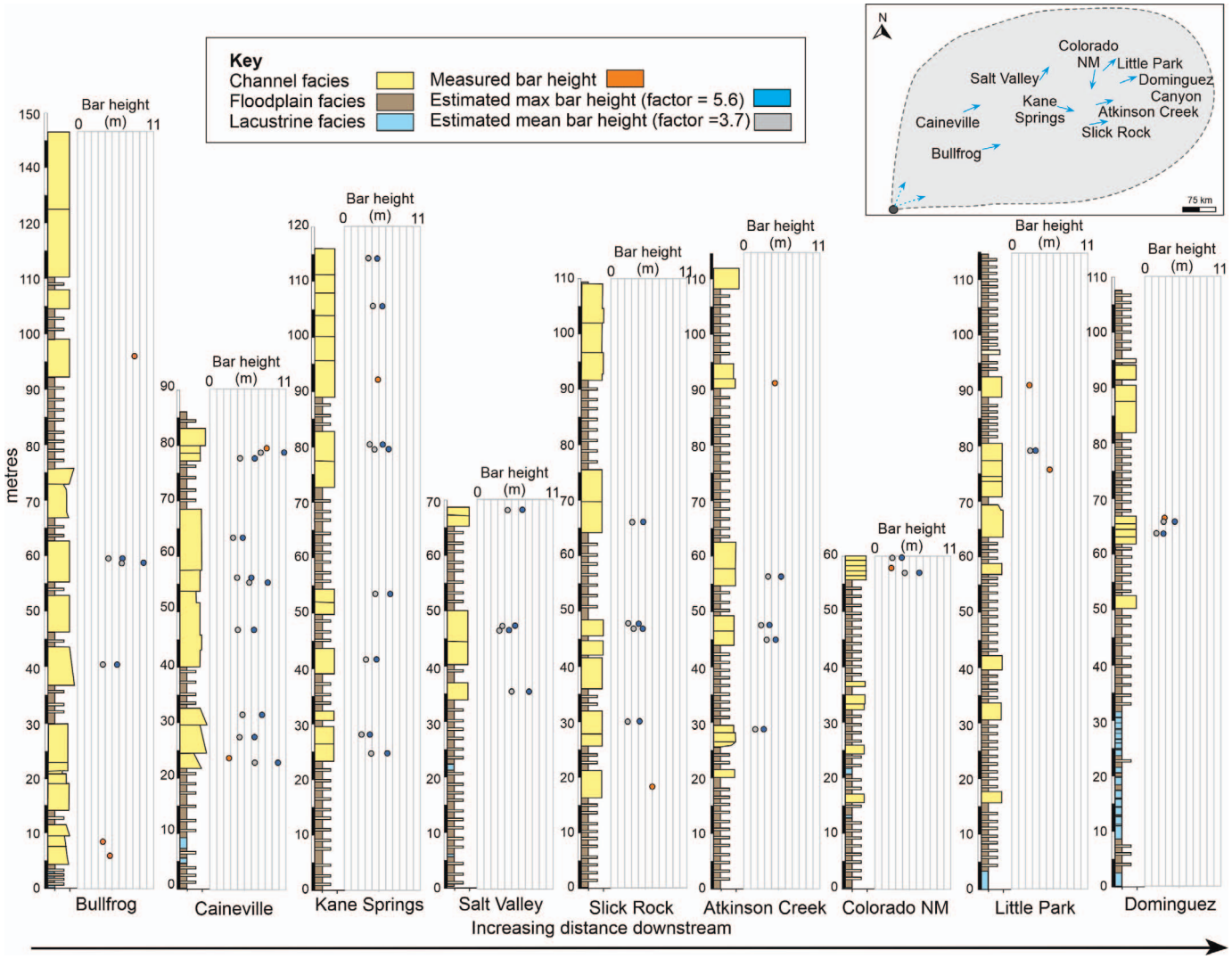

FIG. 2.—Simplified stratigraphic logs of sections studied in the Salt Wash fluvial system with bar heights (measured and calculated) noted. Inset map shows location of each stratigraphic log.

$$A = d_b w_c 0.65 \quad (6)$$

where w_c is channel width. Channel width was estimated using empirical relationships reported in Crane (1982) and Bridge and Mackey (1993) (Table 3). Flow-velocity estimates are obtained from the phase diagrams of Rubin and McCulloch (1980) where the flow depth, grain size, and dominant bedform are known. Channel bodies are composed of predominantly medium sandstone (range from fine to coarse) with dunes as the dominant bedform. Discharge (Q) is calculated by multiplying cross-sectional area (A) by flow velocity (U):

$$Q = UA \quad (7)$$

Nature of Formative Discharge

To investigate the nature of formative discharge in the Salt Wash channel deposits, the coefficient of variation (ratio of standard deviation to mean) of the preserved cross-set thickness (CV(dst)) was calculated. Data on preserved cross-set thickness are taken from Tables 1 and 2. CV(dst) values have been shown to vary systematically with discharge variability, and cross set thickness can therefore yield information on the relative timescales of formative flood variability and bedform adjustment (Leary and Ganti 2019).

RESULTS

Cross-Set Height

The mean cross-set height is shown in Figure 6 (and Tables 1 and 2) and shows a general downstream decrease for both complete and incomplete bar-height datasets; however, there is significant overlap in the data. The range in measured cross-set thickness generally decreases downstream; however, this relationship is only moderate (R^2 of 0.4464) for cross-sets measured from incomplete bar thickness with R^2 of 0.6392 for cross-sets taken from complete bar thicknesses. In general, the lowest values are found in the most distal part of the system; however, low cross-set heights are present across the studied sections. The largest cross-sets are generally found in the proximal and medial areas of the system. The average cross-set thickness for bars with complete thicknesses is 29.5 cm (std dev 9.9) and for incomplete bars it is 35.2 cm (std dev 11.5). The overlap between these values suggests that removal of the tops of incomplete bars through

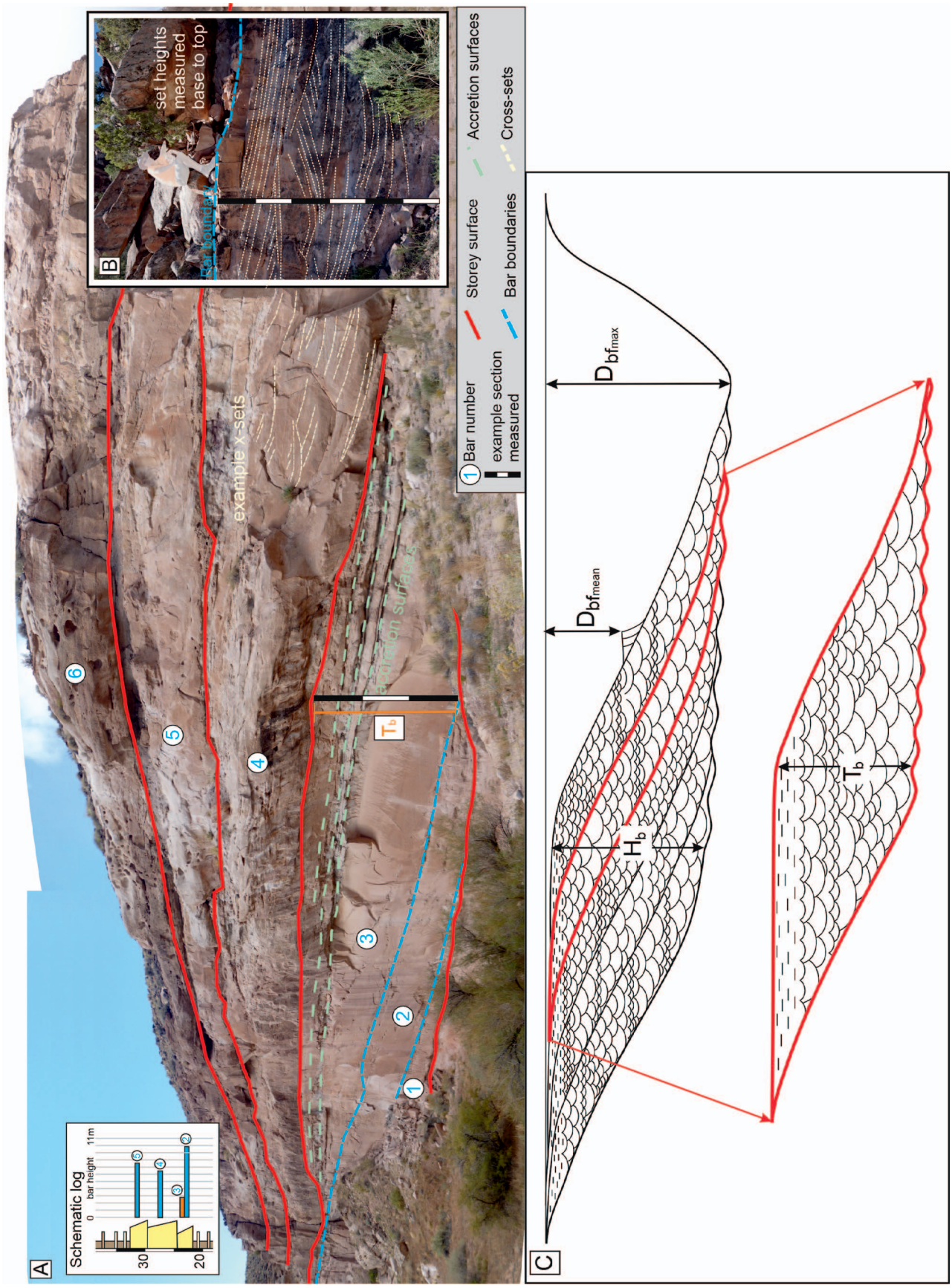

FIG. 3.—**A)** Interpreted image with inset log showing how sandstone bodies were interpreted and measured. Lower story package shows complete preservation of a bar (bar 3) with the scale bar showing how complete bar packages were measured. All other bars are incomplete in this example. **B)** Example image showing how cross-sets were measured in the field in a single bar package. **C)** Schematic diagram illustrating definitions of bar height (H_b), bar thickness (T_b), maximum bankfull depth (D_{bfmax}) and mean bankfull depth (D_{bfmean}). See Bridge (2003) for more detailed explanations.

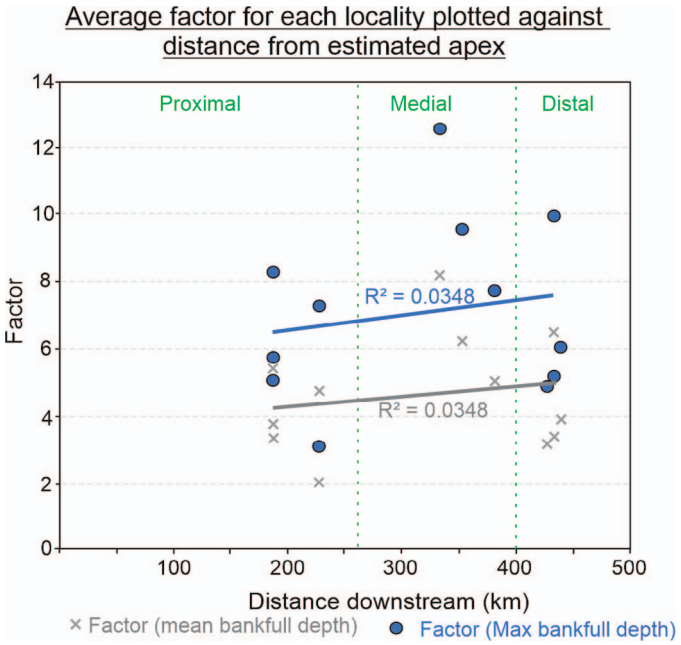

FIG. 4.—Graph showing the calculated average factor for each locality. Note the wide range of factors across the system. See Methods section for details.

erosion has not biased the incomplete bar dataset towards the preservation of larger bedforms in the lower parts of the bars.

Channel Depth

Four channel-depth calculations were conducted on the dataset in which the bar thickness was not measured. The first set of calculations used a factor of 4.6 for mean bankfull depth and 7.1 for max bankfull depth (Fig. 5A), with the second using the minimum (6) and maximum (10) factors of Leclair and Bridge (2001) (Fig. 5B). A broad downstream decrease in channel-depth values can be observed in the dataset derived from both known bar thickness and estimated bar thickness using the mean and maximum Salt Wash factors of 4.6 and 7.1 (orange and blue lines in Fig. 5A, respectively; Tables 1, 2); however, this relationship is relatively weak given R^2 values of 0.2133 (complete bars) and 0.4464 (incomplete bars for all factors). The largest range in channel depths derived from known bar thicknesses is generally found in the most proximal localities, with the smallest range in medial localities. Distal localities generally have the smallest channel depths; however, there is some variability with a mean channel depth of 5.2 m calculated at 427 km downstream (Colorado National Monument). Interestingly, fewer low values are observed in the proximal part of the system, and fewer large values in the distal part in the system when compared to the known-bar-thickness dataset. Overlap between proximal, medial, and distal channel-depth estimates is observed but is not as large as that recorded from the cross-set-height dataset. Despite the overlap, the largest channel depths are generally found in the most proximal localities and the smallest in the most distal localities. A stronger correlation exists between estimated channel depth and distance downstream (R^2 of 0.4464; Fig. 5A) for the channel depths derived from cross-set thicknesses when compared to those derived from known bar thicknesses, possible reasons for which are discussed below.

The same trends described for calculated bar heights using a factor of 4.6 (mean bankfull) and 7.1 (maximum bankfull) can be observed when using Leclair and Bridge minimum and maximum factors (6 and 10 respectively; Fig. 5B). However, as is to be expected, the range in estimated channel depths increases when using a factor of 10, possibly leading to an overestimation of channel depths in the system.

CV(dst)

Values for CV(dst) are illustrated in Figure 7, where they are plotted against distance downstream. Values show a wide range from 0.1 and 1.1; the majority plot between 0.2 and 0.7 with an average of 0.44 (Tables 1, 2). There is no consistent change in CV(dst) downstream. Leary and Ganti (2019) used theoretical analysis and flume experiments on steady and unsteady flows to illustrate that cross-strata with values of CV(dst) $\approx$ 0.88 are likely developed under broad flood hydrographs that show a gradual decline in discharge, whereas flashier flood hydrographs with rapid decreases in flood discharge tend to result in CV(dst) values lower than 0.88. The low CV(dst) values recorded here indicate significant bedform disequilibrium relative to formative flows. Deposition is considered to be associated with rapid decreases in flood discharge likely associated with flashy flood hydrographs.

Paleohydraulics

Channel depths for the Salt Wash fluvial system were calculated for two main datasets: measured bar heights and estimated depths using the Leclair and Bridge (2001) method with factors determined in this study (4.6 for

TABLE 1.—*Data for measured (complete) bars from the Salt Wash fluvial system. Note that values for mean cross-set height and channel depth are uncompacted (see Methods section for details) and the channel-depth calculation utilized the conversion of bar thickness to bar height factor of 0.8.*

Location	Distance Downstream (km)	Factor (Average Max Bankfull)	Factor (Average Mean Bankfull)	Mean Set Thickness Uncompacted (cm)	CV	STDV	Max Channel Depth from Bar Thickness Uncompacted (m)
Caineville	227	3.08	2.00	38.89	0.20	7.86	3.47
	227	7.28	4.73	48.02	0.54	26.11	10.14
Bullfrog	187	5.08	3.30	41.48	0.42	17.22	6.11
	187	5.75	3.74	28.33	0.32	9.12	4.72
	187	8.31	5.40	42.14	0.51	21.65	10.15
Kane Springs	333	12.66	8.23	16.45	0.58	9.56	6.04
Slick Rock	352	9.63	6.26	27.06	0.68	18.48	7.56
Atkinson Creek	381	7.76	5.04	24.51	0.50	12.31	5.51
Little Park	433	10.02	6.52	23.41	0.65	15.17	6.81
	433	5.19	3.38	22.22	0.19	4.22	3.35
CNM	427	4.89	3.18	20.48	0.52	10.70	2.90
Dominguez	439	6.03	3.92	20.79	0.46	9.48	3.64
Avg	-	7.14	4.64	29.48	0.46	13.49	5.87
Stdev	-	2.57	1.67	9.93	0.15	6.09	2.38

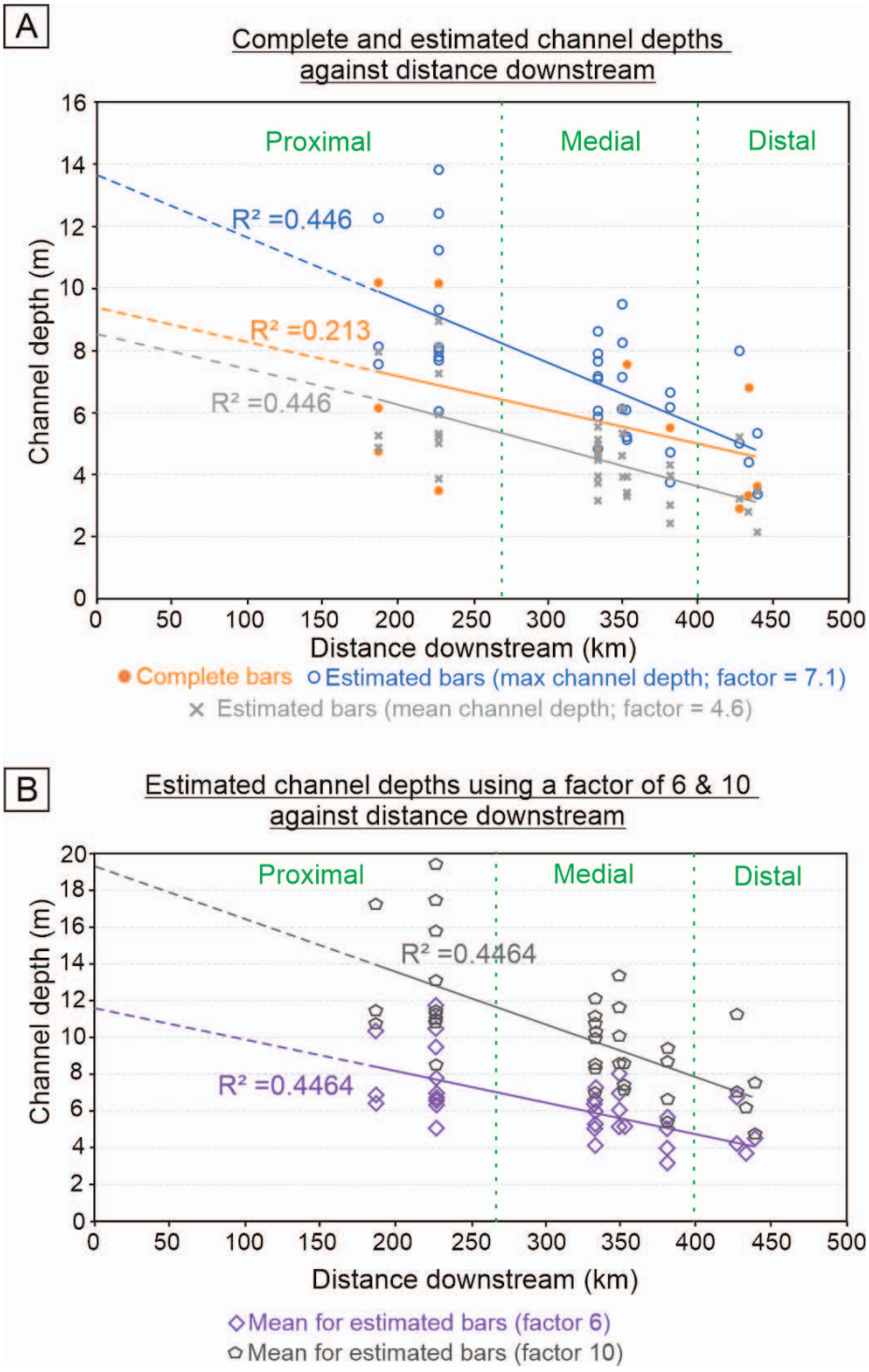

FIG. 5.—**A)** Graph showing measured and calculated channel depths and associated R^2 values. Note calculated mean and maximum channel depths using factors of 4.6 and 7.1, respectively. Gray data points represent the combined dataset of calculated and measured channel depths. Note: the dashed line represents projected trend lines to apex position. **B)** Graph showing estimated channel depths and associated R^2 values using two factors (6 and 10) based on the work of Leclair and Bridge (2001). See Tables 1 and 2 for raw data.

mean bankfull and 7.1 for maximum bankfull). To calculate paleodischarge, channel widths were estimated using the approach of Bridge and Mackey (1993) and Crane (1982). It is noted that there can be significant variation in channel-width estimates depending on channel type (e.g., braided versus meandering). We are confident that previous work utilizing remotely sensed data and outcrop analysis (Hartley et al. 2015; Owen et al. 2015b; Swan et al. 2018) indicates that the fluvial deposits in all of the studied sections (except Bullfrog) record deposition by meandering rivers. As estimated bar heights are generally larger for the datasets in which bar height was unknown (Fig. 5), it is unsurprising that the largest width estimates are derived from this dataset, and those for the known bar heights have the lowest widths (Table 3; Fig. 8A, B). Despite the variations in absolute estimates, all estimates show a downstream decrease in channel width (Fig. 8A, B; Table 3). An average of all datasets was produced to highlight the clear downstream trend with a R^2 of 0.8543 for maximum channel depth (Fig. 8A) and a R^2 of 0.7929 for mean channel depth (Fig. 8B). When assessing the data as a whole it is evident there is some overlap in estimates between proximal, medial, and distal parts of the system.

TABLE 2.—*Data for calculated (incomplete) bars from the Salt Wash fluvial system (see methods section for details).*

Location	Distance Downstream (km)	Mean Set Thickness Uncompacted (cm)	STDV Mean Set	Calcuated Dune Height from Uncompacted Set Thickness (cm)	CV	Calculated Max Channel Depth (× 7.1) (m)	Calculated Mean Channel Depth (× 4.6) (m)	Calculated Channel Depth (× 6) (m)	Calculated Channel Depth (× 10) (m)
Caineville	227	60.19	19.88	174.54	0.33	12.39	8.10	10.47	17.45
	227	39.05	39.27	113.24	1.01	8.04	5.21	6.79	11.32
	227	45.14	29.19	130.90	0.65	9.29	6.02	7.85	13.09
	227	37.92	39.76	109.96	1.05	7.81	5.06	6.60	11.00
	227	29.22	22.78	84.74	0.78	6.02	3.90	5.08	8.47
	227	36.94	7.59	107.14	0.21	7.61	4.93	6.43	10.71
	227	54.44	42.80	157.89	0.79	11.21	7.26	9.47	15.79
	227	39.57	18.28	114.76	0.46	8.15	5.28	6.89	11.48
	227	66.94	25.58	194.14	0.38	13.78	8.93	11.65	19.41
Bullfrog	187	36.72	15.23	106.49	0.41	7.56	4.90	6.39	10.65
	187	39.44	24.03	114.39	0.61	8.12	5.26	6.86	11.44
	187	59.44	20.19	172.39	0.34	12.24	7.93	10.34	17.24
Kane Springs	333	37.08	22.01	107.54	0.59	7.64	4.95	6.45	10.75
	333	23.68	12.00	68.66	0.51	4.87	3.16	4.12	6.87
	333	28.41	11.72	82.40	0.41	5.85	3.79	4.94	8.24
	333	41.73	9.74	121.01	0.23	8.59	5.57	7.26	12.10
	333	38.38	20.60	111.29	0.54	7.90	5.12	6.68	11.13
	333	34.30	11.57	99.46	0.34	7.06	4.58	5.97	9.95
	333	34.79	12.81	100.88	0.37	7.16	4.64	6.05	10.09
	333	29.44	9.77	85.39	0.33	6.06	3.93	5.12	8.54
Salt Valley	349	46.11	20.07	133.72	0.44	9.49	6.15	8.02	13.37
	349	29.56	7.88	85.71	0.27	6.09	3.94	5.14	8.57
	349	34.72	14.46	100.69	0.42	7.15	4.63	6.04	10.07
	349	40.00	7.37	116.00	0.18	8.24	5.34	6.96	11.60
Slick Rock	352	25.28	9.11	73.31	0.36	5.20	3.37	4.40	7.33
	352	29.51	9.39	85.57	0.32	6.08	3.94	5.13	8.56
	352	24.81	6.36	71.96	0.26	5.11	3.31	4.32	7.20
	352	29.57	21.27	85.75	0.72	6.09	3.94	5.14	8.57
Atkinson Creek	381	32.35	17.62	93.80	0.54	6.66	4.31	5.63	9.38
	381	29.90	15.07	86.71	0.50	6.16	3.99	5.20	8.67
	381	22.85	8.64	66.26	0.38	4.70	3.05	3.98	6.63
	381	18.21	4.58	52.79	0.25	3.75	2.43	3.17	5.28
Little Park	433	21.26	10.02	61.65	0.47	4.38	2.84	3.70	6.17
CNM	427	38.78	3.88	112.46	0.10	7.98	5.17	6.75	11.25
	427	24.25	5.58	70.33	0.23	4.99	3.24	4.22	7.03
Dominguez	439	16.32	6.97	47.32	0.43	3.36	2.18	2.84	4.73
	439	25.93	3.49	75.19	0.13	5.34	3.46	4.51	7.52
AVERAGE		35.19	15.85	102.07	0.44	7.25	4.70	6.12	10.21
STDV		11.33	9.86	32.86	0.22	2.33	1.52	1.97	3.29

However, the overlap is present only when considering the different methods for estimating channel width and once average values are calculated, estimates can be clearly split into the proximal, medial, and distal regions of the system. This observation is in line with measurements of channel widths of modern DFSs from satellite imagery analysis (e.g., Weissmann et al. 2015).

To estimate discharge (Q), the average of all width estimates (Fig. 8A; Table 3) was used. Again, discharge estimates derived from known bar thicknesses are lower than those for which the bar thickness has been estimated using Leclair and Bridge (2001) (Fig. 8C). This has resulted in a low R^2 value ($R^2 = 0.2533$) because the range in bar thickness across the system is much lower with differences between most proximal and distal localities being minimal. In contrast, a much stronger correlation is present when estimating Q from the dataset in which bar thicknesses were unknown (and therefore calculated) with an $R^2 = 0.6877$. This is due to the higher range in estimates between proximal and distal with proximal estimates being noticeably higher than the known-bar-thickness dataset (Fig. 8C). There is a degree of overlap in estimated Q between the different domains in the system (proximal, medial, and distal) for both the maximum- and mean-channel-depth datasets. For example, when considering the mean-channel-depth dataset, the upper range of estimates for Q in medial localities (e.g., 580 m^3/s for Salt Valley) can fall within the range of estimates for proximal localities (e.g., 634 m^3/s at Bullfrog 227 km downstream; Fig. 8C; Table 3). Similarly, estimates of Q for medial and distal localities show a general downstream decrease when considering the mean channel dataset, however, there is significant overlap between localities. For example, the lowest Q estimate for a medial locality is 161 m^3/s at 352 km downstream (Slick Rock) and the highest Q estimate for a distal locality is 276 m^3/s for 427 km downstream (Colorado National Monument), although this value is significantly higher than the 60 and 77 m^3/s Q determined for the two other distal localities (Table 3, Fig. 8C). These datasets highlight the significant variability that is present in the system; however, a general downstream trend in Q is present, with highest Q estimates being in the most proximal localities and the lowest in the most distal localities.

DISCUSSION

Estimation of Paleochannel Depth

Channel-depth reconstruction in fluvial systems is important for establishing mean and maximum bankfull flow depths and determining

TABLE 3.—*Dataset used to calculate discharge (Q) for each site on the Salt Wash fluvial system. Note bar heights are uncompacted values (see Methods section for details). Note that the channel-depth calculation utilized the bar-thickness-to-bar-height conversion factor of 0.8. See methods section for details on how discharge was calculated.*

Location	Distance Downstream (km)	Bar Thickness Uncompacted (Channel Depth) (m)	dm to db Conversion (Crane 1982)	Width Estimate (m) (Crane 1982)	Average (m) Crane per site	Width Estimate (m) (Bridge and Mackey 1993)	Average (m) (Bridge and Mackey 1993)	Width Estimate (m) (Bridge and Mackey 1993)	Average (m) (Bridge and Mackey 1993)	Average of Width Measurements (m)	Cross-Sectional Area (m2) (Bhattacharya and MacEachern 2009)	Velocity (m^3/s) (Rubin and McCulluch 1980)	Bankfull Discharge (Q) (m^3/s)
Measured bars													
Caineville	227	3.47	6.09	92.78	301.30	85.57	343.59	113.29	364.58	336.49	759.44	0.80	607.55
	227	10.14	17.79	509.82		601.61		615.88					
Bullfrog	187	6.11	10.72	227.94	296.71	239.42	330.76	276.76	359.37	328.95	1306.66	0.80	1045.33
	187	4.72	8.28	151.28		149.75		184.15					
	187	10.15	17.81	510.93		603.11		617.21					
Kane Springs	333	6.04	10.60	223.83	223.83	234.49	234.49	271.80	271.80	243.38	955.76	0.80	764.60
Slick Rock	352	7.56	13.26	319.40	319.40	352.26	352.26	386.98	386.98	352.88	1733.02	0.80	1386.42
Atkinson Creek	381	5.51	9.67	193.56	193.56	198.55	198.55	235.25	235.25	209.12	749.49	0.80	599.59
Little Park	433	6.81	11.94	270.48	179.00	291.22	185.63	328.06	217.49	194.04	858.37	0.80	686.69
	433	3.35	5.87	87.53		80.05		106.91					
CNM	427	2.90	5.09	69.78	69.78	61.76	61.76	85.36	85.36	72.30	136.42	0.70	95.50
Dominguez	439	3.64	6.38	99.96	99.96	93.19	93.19	122.00	122.00	105.05	248.47	0.80	198.78
Calculated bars (max channel depths; factor = 7.1)													
Caineville	227	12.39	21.74	701.44	463.18	866.84	546.28	845.67	559.60	523.02	4212.89	0.80	3370.31
	227	8.04	14.11	352.56		394.43		426.90					
	227	9.29	16.31	443.95		513.51		536.78					
	227	7.81	13.70	336.47		373.89		407.53					
	227	6.02	10.56	222.37		232.74		270.04					
	227	7.61	13.35	322.85		356.62		391.14					
	227	11.21	19.67	598.09		722.28		721.79					
	227	8.15	14.29	360.13		404.14		436.00					
	227	13.78	24.18	830.78		1052.13		1000.54					
Bullfrog	187	7.56	13.26	319.73	455.26	352.68	533.99	387.39	550.15	513.13	2521.71	0.80	2017.37
	187	8.12	14.25	358.28		401.76		433.77					
	187	12.24	21.47	687.76		847.52		829.28					
Kane Springs	333	7.64	13.40	324.78	324.94	359.06	304.15	393.47	338.95	322.68	1601.47	0.80	1281.18
	333	4.87	8.55	159.12		158.67		193.64					
	333	5.85	10.26	212.66		221.14		258.32					
	333	8.59	15.07	391.82		445.10		474.12					
	333	7.90	13.86	342.97		382.17		415.36					
	333	7.06	12.39	286.84		311.47		347.77					
	333	7.16	12.57	293.39		319.62		355.66					
	333	6.06	10.64	225.07		235.97		273.29					
Salt Valley	349	9.49	16.66	459.25	336.13	533.82	375.52	555.16	407.04	372.90	2301.26	0.80	1841.01
	349	6.09	10.68	226.42		237.59		274.93					
	349	7.15	12.54	292.53		318.55		354.62					
	349	8.24	14.45	366.33		412.11		443.47					
Slick Rock	352	5.20	9.13	176.59	200.11	178.75	206.56	214.75	243.16	216.61	732.80	0.70	512.96
	352	6.08	10.66	225.82		236.87		274.20					
	352	5.11	8.96	171.47		172.84		208.57					
	352	6.09	10.68	226.57		237.77		275.11					
Atkinson Creek	381	6.66	11.68	261.34	176.24	279.98	192.42	317.04	226.98	198.55	859.52	0.70	601.66
	381	6.16	10.80	230.62		242.64		279.99					
	381	4.70	8.25	150.36		148.71		183.05					
	381	3.75	6.58	104.79		98.36		127.85					

TABLE 3.—*Continued.*

Location	Distance Downstream (km)	Bar Thickness Uncompacted (Channel Depth) (m)	dm to db Conversion (Crane 1982)	Width Estimate (m) (Crane 1982)	Average (m) Crane per site	Width Estimate (m) (Bridge and Mackey 1993)	Average (m) (Bridge and Mackey 1993)	Width Estimate (m) (Bridge and Mackey 1993)	Average (m) (Bridge and Mackey 1993)	Average of Width Measurements (m)	Cross-Sectional Area (m2) (Bhattacharya and MacEachern 2009)	Velocity (m^3/s) (Rubin and McCulluch 1980)	Bankfull Discharge (Q) (m^3/s)
Little Park	433	4.38	7.68	134.09	134.09	130.44	130.44	163.35	163.35	142.63	405.81	0.60	243.49
CNM	427	7.98	14.01	348.70	257.01	389.48	277.62	422.25	311.69	282.11	1464.09	0.60	878.45
	427	4.99	8.76	165.32		165.76		201.13					
Dominguez	439	3.36	5.89	88.03	135.94	80.58	133.88	107.53	165.52	145.11	316.87	0.60	190.12
	439	5.34	9.37	183.84		187.18		223.51					
Calculated bars (mean channel depths; factor = 4.6)													
Caineville	227	8.10	14.21	356.66	232.83563	399.68	248.6350985	431.83	282.5206481	254.6637939	1340.559643	0.8	1072.45
	227	5.21	9.14	176.82		179.02		215.03					
	227	6.02	10.56	222.65		233.07		270.37					
	227	5.06	8.87	168.74		169.69		205.27					
	227	3.90	6.84	111.52		105.63		136.02					
	227	4.93	8.65	161.92		161.86		197.02					
	227	7.26	12.74	299.95		327.82		363.57					
	227	5.28	9.26	180.61		183.42		219.61					
	227	8.93	15.67	416.65		477.53		503.97					
Bullfrog	187	4.90	8.59	160.35	228.31881	160.07	242.3585633	195.13	277.1075742	249.2616498	793.6377508	0.8	634.91
	187	5.26	9.23	179.68		182.34		218.49					
	187	7.93	13.91	344.92		384.66		417.71					
Kane Springs	333	4.95	8.68	162.88	162.96027	162.97	138.0432307	198.19	170.7297746	157.2444234	505.6187883	0.8	404.50
	333	3.16	5.54	79.80		72.01		97.53					
	333	3.79	6.65	106.65		100.37		130.11					
	333	5.57	9.77	196.50		202.01		238.81					
	333	5.12	8.98	172.01		173.45		209.21					
	333	4.58	8.03	143.86		141.37		175.17					
	333	4.64	8.14	147.14		145.06		179.14					
	333	3.93	6.89	112.88		107.10		137.66					
Salt Valley	349	6.15	10.79	230.32	168.57647	242.28	170.4351911	279.63	205.026829	181.3461621	725.0753523	0.8	580.06
	349	3.94	6.92	113.55		107.84		138.48					
	349	4.63	8.13	146.71		144.58		178.62					
	349	5.34	9.36	183.72		187.04		223.37					
Slick Rock	352	3.37	5.92	88.56	100.35948	81.13	93.75006859	108.17	122.4773608	105.5289697	231.3022065	0.7	161.91
	352	3.94	6.91	113.25		107.51		138.11					
	352	3.31	5.81	86.00		78.45		105.06					
	352	3.94	6.92	113.63		107.92		138.57					
Atkinson Creek	381	4.31	7.57	131.07	88.387656	127.08	87.33496251	159.69	114.3307017	96.68444009	271.1702523	0.7	189.82
	381	3.99	7.00	115.66		110.13		141.03					
	381	3.05	5.35	75.41		67.50		92.20					
	381	2.43	4.26	52.55		44.64		64.40					
Little Park	433	2.84	4.98	67.25	67.24923	59.20	59.2016988	82.28	82.28137109	69.5774334	128.2583707	0.6	76.96
CNM	427	5.17	9.08	174.88	128.89396	176.77	126.00357	212.68	156.9976286	137.298386	461.6549915	0.6	276.99
	427	3.24	5.68	82.91		75.23		101.31					
Dominguez	439	2.18	3.82	44.15	68.17429	36.57	60.76366491	54.16	83.37296298	70.77030583	100.1217315	0.6	60.07
	439	3.46	6.07	92.20		84.96		112.58					

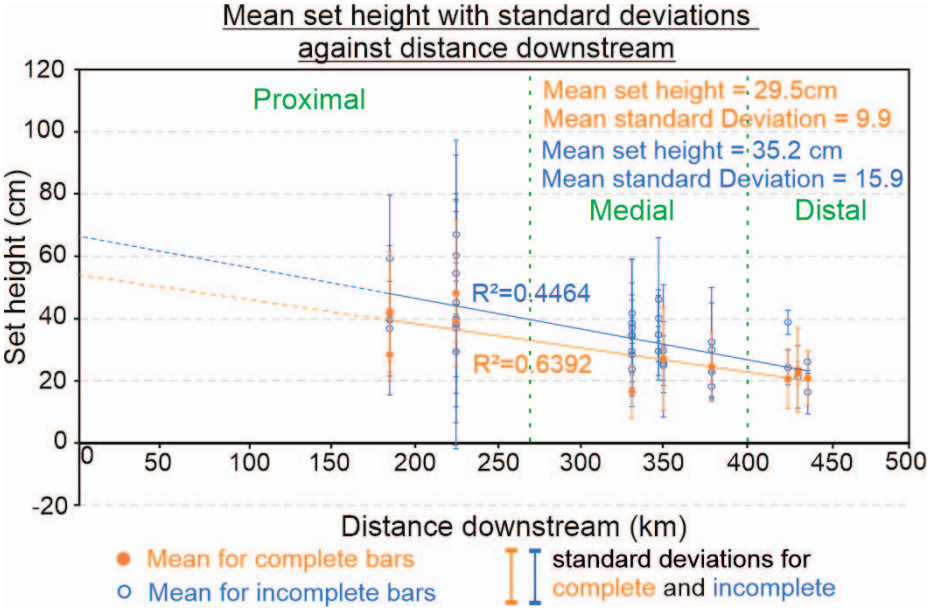

FIG. 6.—Graph showing the mean set heights and associated R^2 values for cross-sets from both measured bars (orange) and incomplete (calculated) bars. Note: dashed lines represent projected trend lines to apex position. See Tables 1 and 2 for raw data.

paleohydraulic parameters as well as predicting likely channel-body dimensions. The methodology established by Leclair and Bridge (2001) has been widely used and applied in the rock record (e.g., Bhattacharya and Tye 2004; Adams and Bhattacharya 2005; McLaurin and Steel 2007). In our analysis of the Salt Wash dataset, we suggest an approach additional to that of Leclair and Bridge to enable estimation of channel flow depth. In particular, if bar heights can be estimated from thicknesses and converted from maximum to mean bankfull flow depth, then determination of the factor to estimate mean flow depth can be used to calibrate flow depths derived from trough cross-set heights. It is interesting to note that the factor of 4.6 estimated here for mean bankfull flow depth is lower than those of Leclair and Bridge (6–10) that were derived from observations on flume experiments and present-day rivers. However, our lower value is in line with recent experimental work that established that whilst dunes developed in flow depths of $>$ 2.5 m have a wide range of heights, they tend to be less than 1/6 of the flow depth (Bradley and Venditti 2017, 2019). If possible, we suggest that an approach that combines measured bar thickness and cross-set heights should be utilized in outcrop studies of fluvial and deltaic channel deposits (e.g., Bhattacharya and Tye 2004) to determine mean and maximum channel flow depth.

Paleohydraulics

Downstream changes in channel presence and grain size have been demonstrated on a number of distributive fluvial systems, such as the Salt Wash (Mullens and Freeman 1957; Owen et al. 2015b), the Miocene Huesca system, Spain (Hirst 1991; Martin et al. 2021), and the Sunnyside Member of the Eocene-age Green River Formation, USA (Wang and Plink-Björklund 2019). In addition, downstream changes in discharge on the modern Pilcomayo River have been documented by Martin-Vide et al. (2014) and active channel width on the modern Bermejo DFS by Weissmann et al. (2015). Yet, systematic changes in paleohydraulic

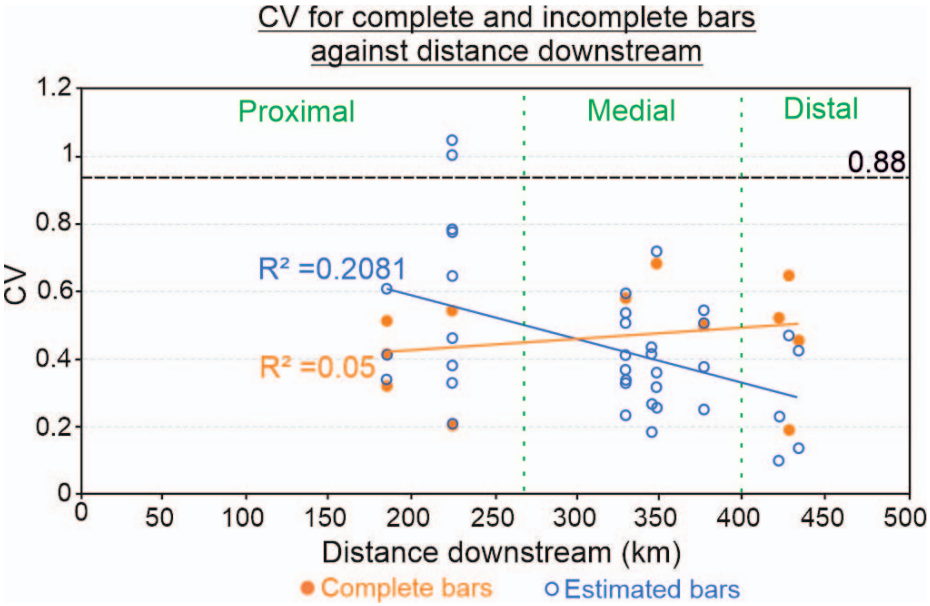

FIG. 7.—Graph showing coefficient of variation (CV) for complete bars and calculated bars. Black dashed line at 0.88 marks the boundary between steady-state and unsteady-state flow (see text for details).

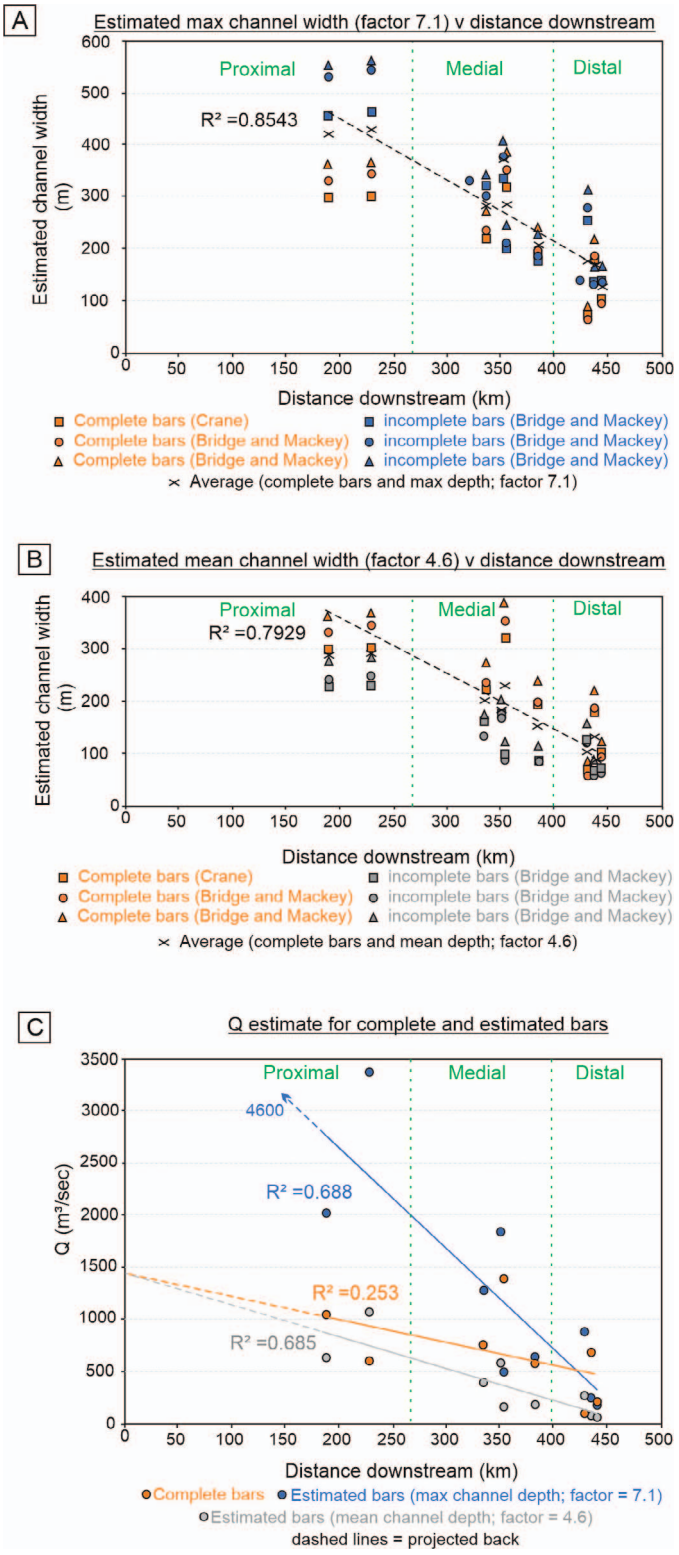

FIG. 8.—**A)** Graph showing estimated channel widths for complete and incomplete bars using a factor of 7.1 (max bankfull). Estimates are shown for a variety of methods (see Methods section and Table 3 for explanation). **B)** Graph showing estimated channel widths for complete and incomplete bars using a factor of 4.6. Estimates are shown for a variety of methods (see Methods section and Table 3 for explanation). **C)** Graph showing estimated average discharge (Q) for each site with associated R^2 values for complete bars (orange) and estimated (blue) bars using a factor of 7.1 and estimated (gray) using a factor of 4.6. Note: dashed lines represent projected trend lines to apex position, and gray crosses show the average discharge for these datasets combined. See Table 3 for raw data.

properties have yet to be documented on any ancient DFS deposit, despite the assumption that these trends are present (e.g., Weissmann et al. 2015). The paleohydraulic properties of the Salt Wash DFS show systematic downstream trends in cross-set height (Fig. 6), bar height, and channel depth (Fig. 5), and estimated channel width and estimated Q (Fig. 8). Downstream loss of discharge is considered to occur on DFSs due to channel bifurcation, infiltration into a sandy substrate, or evapotranspiration (dependent on basin climate), or a combination of these processes (Weissmann et al. 2010, 2013, 2015). The progressive loss of discharge due to a lack of tributary input means that flow competence and volume decrease downstream, resulting in a decrease in the bedload grain size and progressively smaller channels (as documented by Mullens and Freeman 1957; Hirst 1991; Owen et al. 2015b). Additionally, reduced discharge restricts the ability of the channel to erode underlying deposits, which, coupled with an increase in the area available for avulsion, results in a downstream reduction in channel-deposit amalgamation and increasing isolation of channel bodies in floodplain sediment (e.g., Hirst 1991; Owen et al. 2015; Martin et al. 2021).

Whilst the downstream reduction in cross-set height and bar height, and subsequent derivations of channel width, depth, and estimated discharge in the Salt Wash DFS are clear, there is however, important variability in these parameters. Cross-set height values show significant variability and overlap in the data and relatively high standard deviations, particularly at the most proximal sites in the system (Fig. 6; Table 1). Variability of cross-set height may be due to variation in formative flow depth and/or preservation potential. The latter is deemed to be of particular importance in the most proximal part of the system where the greatest degree of reworking by subsequent channels is expected and is supported by the greater degree of channel-deposit amalgamation (Owen et al. 2015b). Variability in flow conditions related to formative channel processes may also account for the range in cross-set-height values. For example, cross-set heights recorded in channel deposits that form due to neck cutoff and progressive channel abandonment will reflect lower formative discharge values than equivalent main-stem-channel deposits. Fluctuations in formative discharge are also indicated by the CV(dst) values (Fig. 7), which range from 0.1 to 1.1 and show no downstream trend. If the measured bedforms were generated at or shortly after peak flood events, then values close to 0.88 would be expected (Leary and Ganti 2019). The wide range in CV(dst) reported here is indicative of more flashy discharge across the entire Salt Wash DFS; as such, it would not be unusual to record a wide range of cross-set and bar-height values leading to significant variability in subsequent derivations of channel width, depth, and discharge. This is in line with the interpretation of the prevailing climate during Salt Wash deposition as semiarid with seasonal precipitation, similar to the African savannah of today (e.g., Demko et al. 2004; Turner and Peterson 2004; Owen et al. 2015b). Flashy (variable) discharge associated with a semiarid climate regime is also supported by the dominance of trough cross-strata as the prevailing bedform (Owen et al. 2015b), although upper-flow-regime structures and large-scale low-angle bedforms suggestive of more flashy dry subtropical systems (e.g., Fielding et al. 2009) are noted but are not prevalent.

Variability in cross-set and bar-height values may also be related to stratigraphic position in the Salt Wash succession, particularly because the system is known to be overall prograding in response to climatic and/or tectonic controls in the catchment area (e.g., Kjemperud et al. 2008; Owen et al. 2017). In a progradational succession, at any given point it would be expected that the hydraulic geometry and discharge of a channel will increase up-section. The distribution of the data collected is shown in Figure 2 with measurements across the entire stratigraphic range from base to top. No significant variability with stratigraphic position was recorded. The lack of correspondence between cross-set and/or bar height and stratigraphic position could be due to a number of reasons. At the small scale, autocyclic switching of avulsive channel belts will lead to significant variability in channel size, as shown by the fact that measurements taken

from nearly equal stratigraphic positions (e.g., at the base or top of the succession: Fig. 2), show a wide range in values that cover much of the dataset. At a larger scale, the migration and/or avulsion of active channel belts across a DFS will produce significant temporal variations in channel dimensions, as documented in the Tista megafan in the Himalayan foreland of India (Chakraborty and Ghosh 2010; Abrahami et al. 2018). Large-scale channel-belt switching across the Salt Wash DFS is also considered to be responsible for sections that deviate from the norm of progradation, with aggradational or retrogradational successions locally developed (Owen et al. 2017). Autocyclic variability is therefore expected and evident at a range of scales in the Salt Wash system and likely accounts for the lack of a coherent up-section change in cross-set and bar-height values. The inherent variability that results from combined autocyclic (channel avulsion and channel-belt switching) and allocyclic (progradation caused by tectonic–climatic changes in the catchment) controls is evident in a number of studies of fluvial systems e.g., Rittersbacher et al., (2014); Kukulski et al. (2013), Owen et al. (2017), Hajek and Straub (2017), Wang and Plink-Bjorkland (2019), and Lyster et al. (2021).

The data presented here highlight the significant spatial and temporal variation in paleohydraulic characteristics recorded in the Salt Wash DFS, including both autocyclic controls related to discharge, channel abandonment, and depth of scour and more regional allocyclic controls such as progradation. To capture this inherent variability, a system-wide study with a significant number of measurements is required and is particularly important in medial deposits. Despite this variability, though, it is clear that meaningful regional trends can be identified in the data, but that a wide spatial and temporal distribution is required, such that studies with more limited datasets may not necessarily identify regional trends.

Paleodischarge and Drainage-Basin Area

The methods utilized here to calculate paleodischarge and to derive drainage-basin size are widely used in the literature (e.g., Bhattacharya and Tye 2004; Davidson and North 2009; Bhattacharya et al. 2016). It is important to note that for a true estimate of drainage-basin area, paleodischarge values must be derived from channel deposits that record the discharge from the whole of the catchment area. For example, in their study of the Ferron delta Bhattacharya and Tye (2004) identified and estimated the discharge for the trunk channel system using a number of approaches. In nondeltaic systems it is important therefore to understand the context of the fluvial system being studied and to consider whether the calculated discharge from studied channel deposits is likely to be representative of the whole of the drainage-basin area. For example, calculations from channels deposited as part of axial or valley-fill fluvial system (Hartley et al. 2018), as with the trunk channels supplying deltas, are likely to encompass all the upstream discharge of a drainage basin and be representative of the whole catchment area. In contrast, as discharge is known to decrease downstream on DFS deposits (Davidson et al. 2013) then unless the studied deposits occur at the apex of the DFS then drainage-basin area will be underestimated. The discrepancy between drainage-basin area and paleodischarge estimates will increase with increasing distance downstream of the apex.

Extrapolating discharge upstream to the apex area would suggest mean bankfull depth discharge values of 1450 m^3/s with a maximum bankfull discharge around 4600 m^3/s (Fig. 8C), which is in line with present-day DFS of similar sizes such as the Pilcomayo in the Andean foreland (discharge values between 3.2 and 5500 m^3/s, Martin-Vide et al. 2014) and Tista (up to 2000 m^3/s, Chakraborty and Ghosh 2010). To accurately reconstruct the drainage-basin area of an entire DFS it is necessary to either have a wide spatial range of data from channels of approximately the same age and demonstrably from the same DFS or be able to reconstruct downstream trends to extrapolate likely discharge values at the apex of the system. Without the spatial context of the studied system being well understood, drainage-basin-area calculations of DFS/megafans based on paleodischarge reconstructions are likely to be significantly underestimated.

A useful predictive aspect of the Salt Wash paleohydrological study is that the spatial distribution of the dataset allows extrapolation of trends that permit the characteristics of the proximal apical area of the DFS to be inferred. The estimated location of the apex area is shown in Figure 1, and approximately 150 km of strata are either unexposed or removed by erosion between the inferred apex point and the closest outcrop of Salt Wash strata (Owen et al. 2015a). Our data indicate that the fluvial system in the apex area would have had an approximate mean and maximum bankfull depth of 9 and 14 m, respectively (Fig. 5A) and a mean bankfull depth discharge of around 1450 m^3/s (Fig. 8), and would have produced mean cross-set heights of between 50 and 70 cm (Fig. 6). Whilst it is noted that there is significant uncertainty associated with these estimates, they do provide a useful approach to predicting likely characteristics of fluvial systems in areas with limited or no data.

CONCLUSIONS

A paleohydraulic analysis has been undertaken on fluvial channel deposits of the Upper Jurassic Salt Wash DFS of the Morrison Formation, SW USA. Channel depth was estimated using two independent methods: 1) cross-set-height values following the methodology of Leclair and Bridge (2001) and 2) preserved bar thickness. Nine localities distributed across the exposed part of the Salt Wash system were studied. Average cross-set height was calculated from 49 bars and compared to measured bar thickness determined from 12 of the studied bars. Calibration of estimates of mean channel depth derived from cross-set heights against maximum channel depth determined from known bar thickness allowed the independent calculation of a factor of 4.6 required to ascertain mean channel depth from bar thickness and 7.1 for maximum channel depth. Calibration against known bar height is useful, because the application of the factors of 6 to 10 identified by Leclair and Bridge (2001) where bar thickness is not known results in a significant range in channel-depth estimates.

Systematic downstream trends in cross-set thickness, bar thickness, and channel depth (mean and maximum), estimated channel width, and estimated Q are recorded with variability and overlap between the proximal to medial, and the medial to distal parts of the DFS. The variability superimposed on the regional downstream trends is attributed to a combination of autocyclic processes such as local variations in discharge, channel abandonment, depth of scour, and channel avulsion as well as more regional-scale channel-belt switching on the DFS together with allocyclic controls such as the overall progradation of the Salt Wash system. An important aspect of this study is the recognition that without the wide spatial distribution of the datasets in this study, regional trends would be difficult to identify and the variability inherent in large scale fluvial systems would predominate.

Formative discharge shows no downstream trend with a wide range in coefficient of variation of preserved cross set thickness indicative of flashy discharge across the entire Salt Wash DFS.

The spatial distribution of the Salt Wash dataset allows extrapolation of trends that permit the characteristics of the proximal apical area of the DFS which is considered to lie $\sim$ 150 km to the southwest of the closest outcrop of Salt Wash strata (Owen et al. 2015a). Our data indicate that the fluvial system in the apex area would have had a mean bankfull depth of 9 m and a bankfull depth discharge of around 1450 m^3/s with mean cross-set heights of between 50 and 70 cm. These estimates are in line with those from modern DFSs of similar scales in the Himalayan and Andean forelands.

ACKNOWLEDGMENTS

We would like to thank AE Janok Bhattacharya and Journal reviewers John Holbrook and W. Lin for their insightful and helpful reviews.

REFERENCES

Abrahami, R., Huyghe, P., Van Der Beek, P., Lowick, S., Carcaillet, J., and Chakraborty, T., 2018, Late Pleistocene–Holocene development of the Tista megafan (West Bengal, India): ^{10}Be cosmogenic and IRSL age constraints: Quaternary Science Reviews, v. 185, p. 69–90.

Adams, M.M., and Bhattacharya, J.P., 2005, No change in fluvial style across a sequence boundary, Cretaceous Blackhawk and Castlegate formations of central Utah, U.S.A: Journal of Sedimentary Research, v. 75, p. 1038–1051.

Allen, J.R.L., 1965, A review of the origin and characteristics of recent alluvial sediments: Sedimentology, v. 5, p. 89–191.

Allen, J.R.L., 1982, Sedimentary Structures: Their Character and Physical Basis, Volume 1: Amsterdam, Elsevier, 663 p.

Bhattacharya, J.P., and MacEachern, J.A., 2009, Hyperpycnal rivers and prodeltaic shelves in the Cretaceous Seaway of North America: Journal of Sedimentary Research, v. 79, p. 184–209.

Bhattacharaya, J.P., and Tye, B., 2004, Searching for modern Ferron analogs and application to subsurface interpretation, *in* Chidsey, T.C., Jr., Adams, R.D., and Morris, T.H., eds., Regional to Wellbore Analog for Fluvial–Deltaic Reservoir Modeling: The Ferron Sandstone of Utah: American Association of Petroleum Geologists, Studies in Geology, v. 50, p. 39–57.

Bhattacharya, J.P., Copeland, P., Lawton, T.F., and Holbrook, J., 2016, Estimation of source area, river paleo-discharge, paleoslope, and sediment budgets of linked deep-time depositional systems and implications for hydrocarbon potential: Earth-Science Reviews, v. 153, p. 77–110.

Bradley, R.W., and Venditti, J.G., 2017, Reevaluating dune scaling relations: Earth-Science Reviews, v. 165, p. 356–376.

Bradley, R.W., and Venditti, J.G., 2019, Transport scaling of dune dimensions in shallow flows: Journal of Geophysical Research, Earth Surface, v. 124, p. 526–547.

Bridge, J.S., 2003, Rivers and Floodplains: Oxford, U.K., Blackwell, 491 p.

Bridge, J.S., and Mackey, S.D., 1993, A revised alluvial stratigraphy model, *in* Marzo, M., and Puigdefabregas, C., eds., Alluvial Sedimentation: International Association of Sedimentologists, Special Publication 17, p. 319–336.

Bridge, J.S., and Tye, B., 2000, Interpreting the dimensions of ancient fluvial channel bars, channels, and channel belts from wireline-logs and cores: American Association of Petroleum Geologists, Bulletin, v. 84, p. 1205–1228.

Chakraborty, T., and Ghosh, P., 2010, The geomorphology and sedimentology of the Tista megafan, Darjeeling Himalaya: implications for megafan building processes: Geomorphology, v. 115, p. 252–266.

Cisernos, J., Best, J., Van Dijk, T., de Almeida, R.P., Amsler, M., Boldt, J., Freitas, B., Galeazzi, C., Huizinga, R., Iannirubertо, M., Ma, H., Nittrouer, J.A., Oberg, K., Orfeo, O., Parsons, D., Szupiany, R., Wang., P and Zhang, Y., 2020, Dunes in the world's big rivers are characterized by low-angle lee-side slopes and a complex shape: Nature Geoscience, v. 13, p. 156–162.

Collinson, J.D., 1978, Vertical sequence and sand body shape in alluvial sequences, *in* Miall, A.D., ed., Fluvial Sedimentology: Canadian Society of Petroleum Geologists, Memoir 5, p. 577–586.

Craig, L.C., Holmes, C.N., Cadigan, R.A., Freeman, V.L., Mullens, T.E., and Weir, G.W., 1955, Stratigraphy of the Morrison and related formations Colorado Plateau Region: U.S. Geological Survey, Bulletin 1009-E, p. 1–52.

Crane, R.C., 1982, A computer model for the architecture of avulsion-controlled alluvial suites [Ph.D. Thesis]: University of Reading, 534 p.

Dal Corso, J., Bernadi, M., Sun, Y., Song, H., Seyfuyllah, L.J., Preto, N., Gianolla, P., Ruffel, A., Kustatscher, E., Roghi, G., Merico, A., Hohn, S., Schmidt, A.R., Marzoli, A., Newton, R.J., Wignall, P.B., and Bentoon, M.J., 2020, Extinction and dawn of the modern world in the Carnian (Late Triassic): Science Advances, v. 6, p. 1–12.

Davidson, S.K., and North, C.P., 2009, Geomorphological regional curves for prediction of drainage area and screening modern analogues for rivers in the rock record: Journal of Sedimentary Research, v. 79, p. 773–792.

Davidson, S.K., Hartley, A.J., Weissmann, G.S., Nichols, G.J., and Scuderi, L.A., 2013, Geomorphic elements on modern distributive fluvial systems: Geomorphology, v. 180–181, p. 82–95.

Demko, T.M., Currie, B.S., and Nicoll, K.A., 2004, Regional paleoclimatic and stratigraphic implications of paleosols and fluvial/overbank architecture in the Morrison Formation (Upper Jurassic), Western Interior, USA: Sedimentary Geology, v. 167, p. 115–135.

Fielding, C.R., and Crane, R.C., 1987, An application of statistical modeling to the prediction of hydrocarbon recovery factors in fluvial reservoir sequences, *in* Ethridge, F.G., Flores, R.M., and Harvey, M.D., eds., Recent Developments in Fluvial Sedimentology: SEPM, Special Publication 39, p. 321–327.

Fielding, C.R., Allen, J.P., Alexander, J., and Gibling, M.R., 2009, A facies model for fluvial systems in the seasonal tropics and subtropics: Geology, v. 37, p. 623–626.

Foreman, B., Heller, P.L., and Clementz, M.T., 2012, Fluvial response to abrupt global warming at the Paleocene–Eocene boundary: Nature, v. 491, p. 92–95.

Hajek, E.A., and Straub, K.M., 2017, Autogenic sedimentation in clastic stratigraphy: Annual Review of Earth and Planetary Sciences, v. 45, p. 681–709.

Hartley, A.J., Weissmann, G.S., Nichols, G.J., and Warwick, G.L., 2010, Large distributive fluvial systems: characteristics, distribution, and controls on development: Journal of Sedimentary Research, v. 80, p. 167–183.

Hartley, A.J., Owen, A.E., Swan, A., Weissmann, G.S., Holzweber, B.I., Howell, J., Nichols, G.D., and Scuderi, L.A., 2015, Recognition and importance of amalgamated sandy meander belts in the continental rock record: Geology, v. 43, p. 679–682.

Hartley, A.J., Owen, A., Weissmann, G.S., and Scuderi, L.A., 2018, Modern and ancient amalgamated sandy meander belt deposits: recognition and controls on development, *in* Ghinassi, M., Colombera, L., Mountney, N.P., Reesink, A.J., and Bateman, M., eds., Fluvial Meanders and Their Sedimentary Products in the Rock Record: International Association of Sedimentologists, Special Publication 48, p. 349–384.

Hirst, J.P.P., 1991, Variations in alluvial architecture across the Oligo-Miocene Huesca fluvial system, Ebro Basin, Spain, *in* Miall, A.D., and Tyler, N., eds., Three-Dimensional Facies Architecture of Terrigenous Clastic Sediments and Its Implications for Hydrocarbon Discovery and Recovery: SEPM, Concepts in Sedimentology and Paleontology, v. 3, p. 111–121.

Keogh, K.J., Martinus, A.W., and Osland, R., 2007, The development of fluvial stochastic modelling in the Norwegian oil industry: a historical review, subsurface implementation and future directions: Sedimentary Geology, v. 202, p. 249–268.

Kjemperud, A.V., Schomaker, E.R., and Cross, T.A., 2008, Architecture and stratigraphy of alluvial deposits, Morrison Formation (Upper Jurassic), Utah: American Association of Petroleum Geologists, Bulletin, v. 92, p. 1055–1076.

Kukulski, R.B., Hubbard, S.M., Moslow, T.F., and Keegan Raines, M. 2013, Basin-scale stratigraphic architecture of upstream fluvial deposits: Jurassic–Cretaceous foredeep, Alberta Basin, Canada: Journal of Sedimentary Research, v. 83, p. 704–722.

Leary C.P., and Ganti, V., 2019, Preserved fluvial cross strata record bedform disequilibrium dynamics: Geophysical Research Letters, v. 47, p. 1–12.

Leclair, S.F., 2002, Preservation of cross-strata due to the migration of subaqueous dunes: an experimental investigation: Sedimentology, v. 49, p. 1157–1180.

Leclair, S.F., and Bridge, J.S., 2001, Quantitative interpretation of sedimentary structures formed by river dunes: Journal of Sedimentary Research, v. 71, p. 713–716.

Leclair, S.F., Bridge, J.S., and Wang, F., 1997, Preservation of cross-strata due to migration of subaqueous dunes over aggrading and non-aggrading beds: comparison of experimental data with theory: Geoscience Canada, v. 24, p. 55–66.

Leeder, M.R., 1973, Fluviatile fining-upward cycles and the magnitude of paleochannels: Geological Magazine, v. 110, p. 265–276.

Lorenz, J.C., Heinze, D.M., Clark, J.A., and Searls, C.A., 1985, Determination of widths of meander-belt sandstone reservoirs from vertical downhole data, Mesaverde Group, Piceance Creek Basin, Colorado: American Association of Petroleum Geologists, Bulletin, v. 69, p. 710–721.

Lu, J., Cook, P.J., Hosseini, S.A., Yang, C., Ramanak, K.D., Zhang, T., Freitfeld, B.M., Smyth, R.C., Zeng, H., and Hovorka, S.D., 2012, Complex fluid flow revealed by monitoring CO_2 injection in a fluvial formation: Journal of Geophysical Research, v. 117, p. 1–13.

Lyster, S., Whittaker, A.C., Hampson, G.J., Hajek, E.A., Allinson, P.A., and Lathrop, B.A., 2021, Reconstructing the morphologies and hydrodynamics of ancient rivers from source to sink: Cretaceous Western Interior Basin, Utah, USA: Sedimentology, v. 68, p. 2854–2886.

Macdonald, A.M., Bonsor, H.C., Ahmed, K.M., Burgess, W.G., Basharat, M., Calaw, R.C., Dixit, A., Foster, S.S.D., Gopal, K., Lapworth, D.J., Lark, R.M., Moench, M., Mukkherjee, A., Rao, M.S., Shamsudduha, M., Smith, L., Taylor, R.G., Tucker, J., Van Steenbergen, F., and Yadav, S.K., 2016, Groundwater quality and depletion in the Indo-Gangetic Basin mapped from in situ observations: Nature Geoscience, v. 9, p. 762–766.

Martin, B., Owen, A., Nichols, G.J., Hartley, A.J., and Williams, R.D., 2021, Quantifying downstream, vertical and lateral variation in fluvial deposits: implications from the Huesca distributive fluvial system: Frontiers in Earth Science, v. 8, article 564017, p. 1–19.

Martín-Vide, J.P., Amarilla, M., and Zárate, F.J., 2014, Collapse of the Pilcomayo River: Geomorphology, v. 205, p. 155–163.

Mather, A.E., 1993, Basin inversion: some consequences for drainage evolution and alluvial architecture: Sedimentology, v. 40, p. 1069–1089.

McLaurin, B.T., and Steel, R.J., 2007, Architecture and origin of an amalgamated fluvial sheet sand, lower Castlegate Formation, Book Cliffs, Utah: Sedimentary Geology, v. 197, p. 291–311.

Mijnssen, F.C.J., 1997, Modelling of sandbody connectivity in the Schooner Field, *in* Ziegler, K., Turner, P., and Daines, S.R., eds., Petroleum Geology of the Southern North Sea: Future Potential: Geological Society of London, Special Publication 123, p. 169–180.

Moscariello, A., 2005, Exploration potential of the mature Southern North Sea basin margins: some unconventional plays based on alluvial and fluvial fan sedimentation models, *in* Dore, A.G., and Vining, B., eds., Petroleum Geology: North-West Europe and Global Perspectives: 6th Petroleum Geology Conference, The Geological Society of London, Proceedings, p. 595–605.

Mullens, T.E., and Freeman, V.L., 1957, Lithofacies of the Salt Wash Member of the Morrison Formation, Colorado Plateau: Geological Society of America, Bulletin, v. 68, p. 505–526.

Owen, A., Jupp, P.E., Nichols, G.J., Hartley, A.J., Weissmann, G.S., and Sadykova, D., 2015a, Statistical estimation of the position of an apex: application to the geological record: Journal of Sedimentary Research, v. 85, p. 142–152.

Owen, A., Nichols, G.J., Hartley, A.J., Weissmann, G.S., and Scuderi, L.A., 2015b, Quantification of a distributive fluvial system: the Salt Wash DFS of the Morrison Formation, SW USA: Journal of Sedimentary Research, v. 85, p. 544–561.

Owen, A., Nichols, G.J., Hartley, A.J., and Weissmann, G.S., 2017, Vertical trends within the prograding Salt Wash distributive fluvial system, SW United States: Basin Research, v. 29, p. 64–80.

Peterson, F., 1980, Sedimentology of the Uranium-bearing Salt Wash Member and Tidwell unit of the Morrison Formation in the Henry and Kaiparowits Basin, Utah: Utah Geological Association, Publication 8, p. 305–322.

Peterson, F., 1984, Fluvial sedimentology on a quivering craton: influence of slight crustal movements on fluvial processes, Upper Jurassic Morrison Formation, Western Colorado Plateau: Sedimentary Geology, v. 38, p. 21–49.

Rittersbacher, A., Howell, J.A., and Buckley, S.J., 2014, Analysis of fluvial architecture in the Blackhawk Formation, Wasatch Plateau, Utah, U.S.A. using large 3D photorealistic models: Journal of Sedimentary Research, v. 84, p. 72–87.

Robinson, J.W., and McCabe, P.J., 1997, Sandstone-body and shale-body dimensions in a braided fluvial system: Salt Wash Sandstone Member (Morrison Formation), Garfield County, Utah: American Association of Petroleum Geologists, Bulletin, v. 81, p. 1267–1291.

Robinson, J.W., and McCabe, P.J., 1998, Evolution of a braided river system: the Salt Wash Member of the Morrison Formation (Jurassic) in southern Utah, *in* Shanley K.W., and McCabe P.J., eds., Relative Role of Eustasy, Climate, and Tectonism in Continental Rocks: SEPM, Special Publication 59, p. 93–107.

Rubin, D.M., and McCulloch, D.S., 1980, Single and superimposed bedforms: a synthesis of San Francisco Bay and flume observations: Sedimentary Geology, v. 26, p. 207–231.

Swan, A., Hartley, A.J., Owen, A., and Howell, J., 2018, Reconstruction of a sandy point-bar deposit: implications for fluvial facies analysis, *in* Ghinassi, M., Colombera, L., Mountney, N., Reesink, A.J., and Bateman, M., eds., Fluvial Meanders and Their Sedimentary Products in the Rock Record: International Associations of Sedimentologists, Special Publication 48, p. 445–474.

Turner, C.E., and Peterson, F., 2004, Reconstruction of the Upper Jurassic Morrison Formation extinct ecosystem: a synthesis: Sedimentary Geology, v. 167, p. 309–355.

Tyler, N., and Ethridge, F.G., 1983, Fluvial architecture of Jurassic Uranium-bearing sandstones, Colorado Plateau, Western United States, *in* Collinson J.D., and Lewin, J., eds., Modern and Ancient Fluvial Systems: International Associations of Sedimentologists, Special Publication 6, p. 533–547.

Van Dijk, W.M., Densome, A.L., Sinha, R., Singh, A., and Voller, V.R., 2016, Reduced-complexity probabilistic reconstruction of alluvial aquifer stratigraphy, and application to sedimentary fans in northwestern India: Journal of Hydrology, v. 541, p. 1241–1257.

Wang, J., and Plink-Björklund, P., 2019, Stratigraphic complexity in fluvial fans: lower Eocene Green River Formation, Uinta Basin, USA: Basin Research, v. 31, p. 892–919.

Willems C.J.L., Hamidreza, M.N., Wletje, G.J., Donsellaa, M.E., and Bruhn, D.F., 2015, Influence of fluvial sandstone architecture on geothermal energy production: World Geothermal Conference, Melbourne Australia, Proceedings, p. 1–12.

Weissmann, G.S., Zhang, Y., Labolle, E.M., and Fogg, G.E., 2002, Dispersion of groundwater age in an alluvial aquifer system: Water Resource Research, v. 38, p. 13–16.

Weissmann, G.S., Hartley, A.J., Nichols, G.J., Scuderi, L.A., Olsen, M., Buelher, H., and Banteah, R., 2010, Fluvial form in modern continental sedimentary basins: distributive fluvial systems: Geology, v. 38, p. 39–42.

Weissmann, G.S., Hartley, A.J., Scuderi, L.A., Nichols, G.J., Davidson, S.K., Owen, A., Atchley, S.C., Bhattacharaya, P., Chakraborty, T., Ghosh, P., Nordt, L.C., Michel, L., and Tabor, N.J., 2013, Prograding distributive fluvial systems: geomorphic models and ancient examples, *in* Dreise, S.G., Nordt, L.C., and McCarthy, P.J., eds., New Frontiers in Paleopedology and Terrestrial Paleoclimatology: SEPM, Special Publication 104, p. 131–147.

Weissmann, G.S., Hartley, A.J., Scuderi, L.A., Nichols, G.J., Owen, A., Wright, S., Feicia, A.L., Holland, F., and Anaya, F.M.L., 2015, Fluvial geomorphic elements in modern sedimentary basins and their potential preservation in the rock record: a review: Geomorphology. v. 50, p. 187–219.

Wernike, B., 2011, The California River and its role in carving Grand Canyon: Geological Society America, Bulletin, v. 123, p. 1288–316.

Yalin, M.S., 1964, Geometrical properties of sand waves: American Society of Civil Engineers, Journal of the Hydraulics Division, Proceedings, v. 90, HY5, Part 1, p. 105–119.

Received 21 May 2021; accepted 22 February 2022.